

# BEAM DYNAMICS SIMULATIONS FOR THE ESS-BILBAO H<sup>-</sup> ION SOURCE\*

D. Fernández-Cañoto<sup>†</sup>, I. Bustinduy, Z. Izaola, J. Feuchtwanger,  
M. Egúiraun, J. L. Muñoz, I. Rodríguez, and F. J. Bermejo.  
ESS-Bilbao, Zamudio 48170, Bizkaia, Spain

## Abstract

Beam dynamics simulations are performed for the hydrogen negative ion source (ISHN) extraction system of the ESS-Bilbao research accelerator facility. The calculations are performed as a function of platform and extraction potentials, extracted beam current, and the Penning angle. It is expected that calculations will help, not only to improve the extraction system geometry, but its modus operandi.

## INTRODUCTION

The ISHN extraction system of the ESS-Bilbao research accelerator facility will extract H<sup>-</sup> beams with high current and low emittance [1]. A Penning type ion source, similar to the one installed for the ISIS front-end [2], produces the plasma from an electric discharge in between a molybdenum cathode and an anode, after injecting Hydrogen gas and cesium vapor. The electric discharge is fed by a 800 V at 10 mA and 2 A at 80 V DC power supply, and a 100 A high current discharge power supply which provides 1 ms pulses at 50 Hz.

Beam dynamic simulations are analyzed at two different positions related to diagnostic devices currently operating in the extraction column; a DC Current Transformer (DCCT) placed at  $z_{\text{dct}} = 243.5$  mm; and a pepperpot placed at  $z_{\text{pot}} = 973.5$  mm.

## ISHN EXTRACTION SYSTEM

Figure 1 illustrates main elements and parameters of the ISHN extraction system used in these simulations.

A planar rectangular aperture electrode set at a potential of  $V_p$  and placed at  $z = 0$  separates the ion source from the extraction system. The negative ions are extracted throughout a  $10 \times 0.6$  mm<sup>2</sup> rectangular slit in the middle of the electrode. Downstream, it follows a rectangular jaw extraction electrode and a cooled trumpet-shape device working also as a cesium trap. These two extraction system elements are set at the same potential,  $V_{\text{ext}}$ , and both play a crucial role not only in the beam extraction and acceleration process, but also as optical lenses for particle trajectories. Ions are accelerated in a first step at  $qV_{\text{ext}}$  throughout the  $g_1$  extraction gap from  $z = 0$  to  $z = 5.5$  mm. Then, the beam is accelerated from  $qV_{\text{ext}}$  to  $qV_p$  throughout the  $g_2$  post-accelerating gap from  $z = 114.5$  to  $z = 143.4$  mm.

Right after the post-accelerating gap, it follows a post acceleration electrode assembly positioned from  $z = 143.4$  to  $z = 186.4$  mm, consisted of a suppressor electrode and two grounded electrodes.

To stabilize the plasma production, two FeNdB N48 Penning permanent magnets are placed parallel to the aperture plate. These magnets are designed to produce a transverse magnetic flux density of  $B_x \approx -0.22$  T at  $(x, y, z) = (0, 0, 0)$ . This field has also an influence in the extracted beam in such a way that the Lorentz magnetic force,  $\mathbf{F}$ , acting on an ion of charge  $q_i$ , traveling at velocity  $\mathbf{v}$  can be expressed as:

$$\mathbf{F} = q_i \cdot (\mathbf{v} \times \mathbf{B}). \quad (1)$$

The vertical component of  $\mathbf{F}$ ,  $F_y$ , arises as a result of the cross product between  $v_z$  and  $B_x$ , and it is compensated by inclining the aperture plate and the extraction jaw electrode a certain Penning angle,  $\theta_P$ , theoretically estimated from the following relationship:

$$\theta_P = \arcsin\left(\frac{L_P}{R}\right), \quad (2)$$

being  $L_P$  the magnet half length and  $R = \sqrt{2m_i V_{\text{ext}}/q_i/B_x}$  the Larmor gyroradius ( $m_i$  is the mass of the ion).

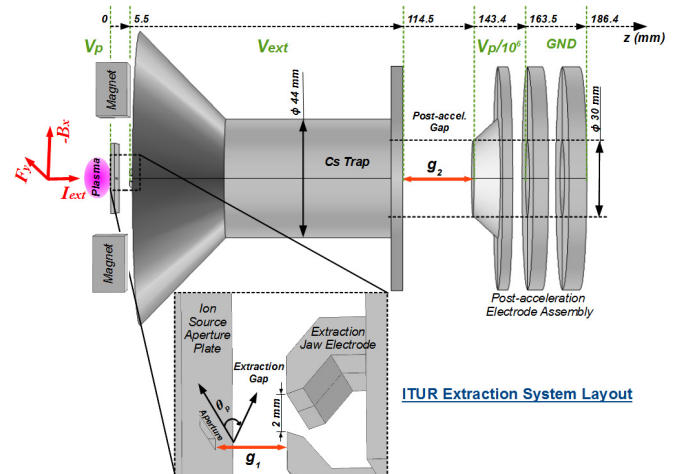


Figure 1: Layout of the ISHN extraction system and its main parameters.

\* Work supported by ESS-Bilbao

<sup>†</sup> david.fernandez@essbilbao.org

## BEAM DYNAMICS

The General Particle Tracer (GPT) code is used to perform the multiparticle dynamics simulations [3]. The 3D electric and magnetic fields are calculated with the COMSOL multiphysics software [4]. The fields are then imported into the GPT code and beam parameters are analyzed at both  $z_{\text{dcct}}$  and  $z_{\text{pot}}$ . The input beam is described with a rectangular particle distribution of about 3700 macroparticles in a Gaussian distribution parallel to the slit aperture and with the same area. To avoid uncertainties with the zero-fields close to the source surface, the input particle distribution is separated 0.5 mm from the aperture plate [5].

Transverse physical boundaries of the extraction system must be included in the simulations to track the loss of particles: the horizontal open ended edges of the extraction jaw electrode delimited from  $x > [-1, 1]$  mm by considering  $y = [-\infty, \infty]$  mm at  $z = 5.5$  mm (as seen in the insert of Figure 1); the  $r_{\text{ap}} = 22$  mm aperture radius relative to the Cs trap found from  $z = 43.9$  to  $z = 114.5$  mm, and the  $r_{\text{ap}} = 15$  mm aperture radius of its support plate located at  $z = 114.5$  mm; the  $r_{\text{ap}} = 15$  mm post-acceleration electrode assembly radial wall limits found from  $z = 143.4$  to  $z = 186.4$  mm. Physical boundaries found within the diagnostics box such as the quadrupole inner walls with  $r_{\text{ap}} = 30.58$  mm found from  $z = 441.5$  to  $z = 513.5$  mm; the dipole rectangular boundaries of width equal to 127 mm and height of 60 mm from  $z = 540.5$  to  $z = 652.5$  mm, and the pepperpot boundaries as width and height equal to 120 mm at  $z_{\text{pot}} = 973.5$  mm are also included [6].

Simulations are performed with  $V_p$  fixed at the common operating potential of  $-35$  kV.  $V_{\text{ext}}$ ,  $\theta_P$ , and  $I_{\text{ext}}$  are parametrically swept within a convenient range of values. In particular,  $I_{\text{ext}}$  is simulated from 5 to 35 mA in 5 mA steps.  $V_{\text{ext}}$  is varied from 10 to 18 kV in 1 kV steps and  $\theta_P$  from 5.5 to 12.5 deg in 0.5 deg steps. Simulations do not include space charge neutralization, multi charge state input beam or the quadrupole and dipole fields (they are not currently used).

The optimum beam parameters are obtained at  $V_{\text{ext}} = 16$  kV, and consequently, results in the following subsections are strictly analyzed at this particular value.

### Lost particles

Figure 2 shows the 2D maps relative to the percentage of lost particles,  $LP$ , calculated at  $z_{\text{dcct}}$  and  $z_{\text{pot}}$  as a function of  $I_{\text{ext}}$  and  $\theta_P$ . At low  $I_{\text{ext}}$  the difference between the  $LP$  at  $z_{\text{dcct}}$  and  $z_{\text{pot}}$  is quite noticeable, and  $LP$  becomes more similar when  $I_{\text{ext}}$  is further increased.

Figure 3 shows  $LP$  as a function of  $z$  for several beam currents  $I_{\text{ext}}$  of 5, 15, 25, and 35 mA, and with the aperture plate set at  $\theta_P = 8.0$  deg. At  $I_{\text{ext}} = 5$  mA, only about 3% of particles would be lost before the DCCT. Unfortunately, even at this low current more than 40% of the particles would be lost by hitting the quadrupole and dipole walls. Once the beam current is increased up to  $I_{\text{ext}} = 15$  mA the

### 05 Beam Dynamics and Electromagnetic Fields

#### D01 Beam Optics - Lattices, Correction Schemes, Transport

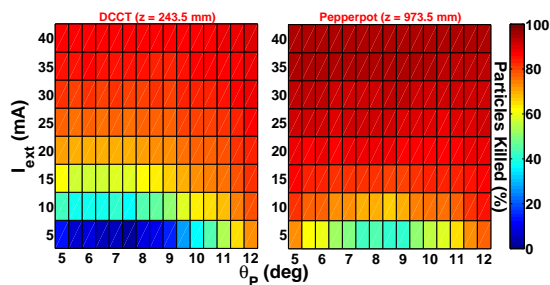


Figure 2:  $LP$  calculated at  $z_{\text{dcct}}$  and  $z_{\text{pot}}$  as a function of  $I_{\text{ext}}$  and  $\theta_P$  for a  $V_{\text{ext}} = 16$  kV.

beam divergence increases and particles start to be lost at the end part of the Cs trap, such a way that 59% of the whole beam is lost before the DCCT, and up to a 82% of the total before the pepperpot. At  $I_{\text{ext}} = 25$  mA, particles would start to hit the walls of the extraction jaw electrode, and 76% of the beam is lost before the DCCT, and only the 10% would reach the pepperpot. At  $I_{\text{ext}} = 35$  mA, particles would be lost almost everywhere and only a 6% of the beam would reach the pepperpot. It is noticeable that at any  $I_{\text{ext}}$  a considerable number of particles would be lost within the quadrupole and dipole walls.

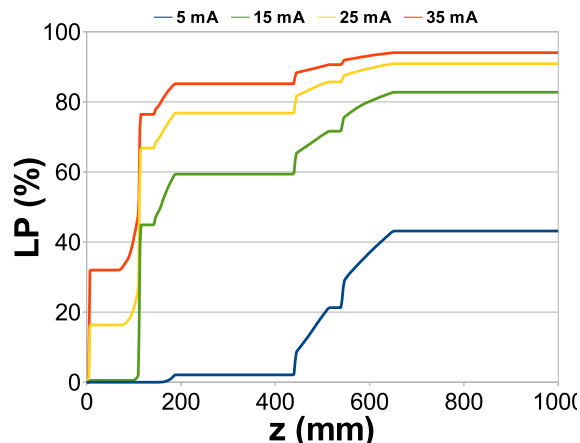


Figure 3:  $LP$  as a function of  $z$  considering  $V_{\text{ext}} = 16$  kV,  $\theta_P = 8.0$  deg, and  $I_{\text{ext}}$  equal to 5, 15, 25, and 35 mA.

### Beam profile and emittances

Figure 4 illustrates the beam transverse dimensions,  $x_{\text{max}}$  and  $y_{\text{max}}$ , calculated at  $z_{\text{dcct}}$  and  $z_{\text{pot}}$  as a function of  $\theta_P$  and  $I_{\text{ext}}$ . In general, at low  $I_{\text{ext}}$ ,  $x_{\text{max}}$  is larger than  $y_{\text{max}}$ , but once  $I_{\text{ext}}$  is increased,  $y_{\text{max}}$  grows more significantly than  $x_{\text{max}}$ .

Figure 5 shows rms transverse emittances calculated at  $z_{\text{dcct}}$  and  $z_{\text{pot}}$  as a function of  $\theta_P$  and  $I_{\text{ext}}$ . In general, rms normalized emittances,  $\epsilon_{\text{rms}}$ , are below  $0.2 \pi$ -mm-mrad due to the large amount of particles lost once the beam current is increased just a few mA.

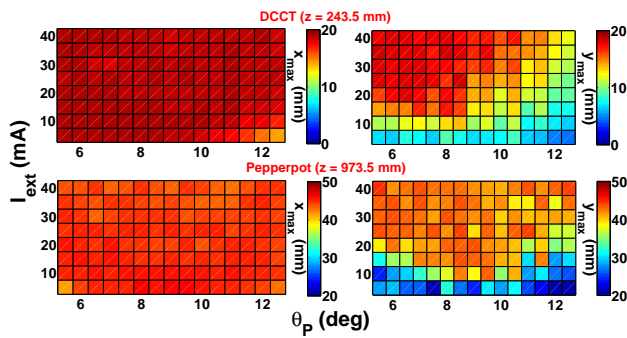


Figure 4:  $x_{\max}$  and  $y_{\max}$  calculated at  $z_{\text{dcct}}$  and  $z_{\text{pot}}$  positions as a function of  $I_{\text{ext}}$  and  $\theta_P$  for  $V_{\text{ext}} = 16$  kV.

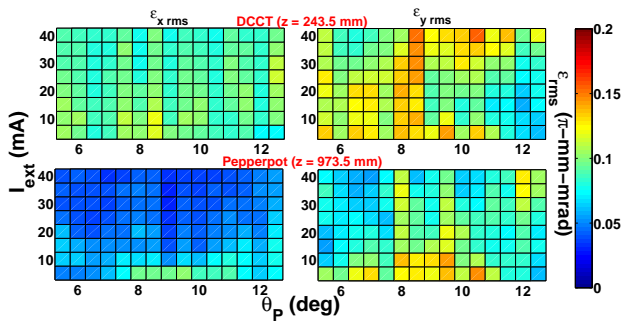


Figure 5: Normalized  $rms$  emittances calculated at  $z_{\text{dcct}}$  and  $z_{\text{pot}}$  as a function of  $I_{\text{ext}}$  and  $\theta_P$  for a  $V_{\text{ext}} = 16$  kV.

### Optimum case

Table 1 gives the best beam parameters for the optimum case which is obtained with  $V_{\text{ext}} = 16$  kV,  $I_{\text{ext}} = 5$  mA and  $\theta_P = 8.0$  deg. By using Eq. (2) and substituting  $V_{\text{ext}}$  and  $B_x$ , a theoretic value of  $\theta_P = 8.57$  deg is calculated. This value is very similar to the one predicted from beam dynamics simulations.

Beam Parameters	$z_{\text{dcct}}$	$z_{\text{pot}}$
$x_{\max}$ [mm]	18.91	45.93
$y_{\max}$ [mm]	8.76	31.78
$\epsilon_{x\text{rms}}$ [ $\pi$ -mm-mrad]	0.1020	0.0938
$\epsilon_{y\text{rms}}$ [ $\pi$ -mm-mrad]	0.1348	0.1225
Lost particles [%]	3	43

Table 1: Beam parameters obtained for the optimum case.

Figure 6 gives the transverse phase space diagrams and beam profiles at  $z_{\text{dcct}}$  and  $z_{\text{pot}}$ . The density maps are designed in basis to the  $(x, x')$  pairs of dots, and normalized to the maximum value. The beam size is larger in the  $x$ -plane than in the  $y$ -plane, and has a perceptible vertical offset at  $z_{\text{pot}}$ . The  $(y, y')$  phase space diagram indicates higher rms emittances than the  $(x, x')$  (see Table 1). Significant differences between the transverse emittance values from similar Penning sources [7] are expected because of beam extraction throughout a rectangular slit.

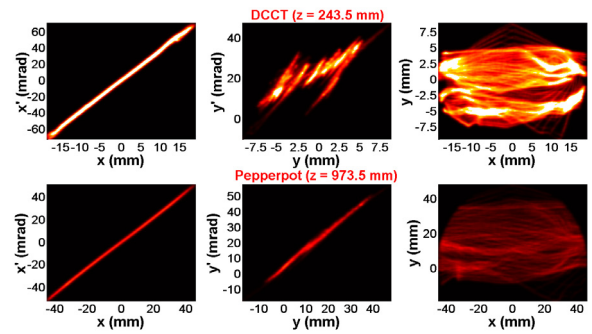


Figure 6: Transverse phase space and beam profile diagrams calculated at  $z_{\text{dcct}}$  and  $z_{\text{pot}}$  for the optimum case.

## CONCLUSIONS

Beam parameters were reasonably acceptable only at low beam currents, where almost the whole beam is able to reach the DCCT; but, unfortunately, a remarkable amount of particles are still lost at the quadrupole and dipole walls. Once the current is increased particles start to be lost at the extraction jaw electrode, the Cs trap, the postaccelerating electrode system, and the quadrupole and dipole boundaries; such that only a small percentage of the initial beam could be successfully transported up to the pepperpot. Therefore, if a high current beam needs to be extracted under optimum conditions, specific parts of the ISHN extraction system directly related to beam optics would have to be redesigned.

## ACKNOWLEDGMENTS

The authors would like to thank Dan Faircloth and Alan Letchford from ISIS for explaining crucial aspects of the beam extraction process in a Penning type ion source.

## REFERENCES

- [1] F. J. Bermejo et al., A Test Stand for Ion Sources of Ultimate Reliability, NIBS08 Conference, Provence, France, September (2008).
- [2] R. Sidlow et al., Operational Experience of Penning  $H^-$  Ion Sources at ISIS, Proceedings of EPAC (1996).
- [3] M.J. de Loos and S.B. van der Geer, Nucl. Instr. and Meth. in Phys. Res. B, Vol. 139, pp. 481 (1997).
- [4] Comsol Multiphysics Package, <http://www.comsol.com/>.
- [5] Stanley Humphries Jr., J.Comp.Phys. 204, 587-597 (2005).
- [6] I. Bustinduy et al., First Simulation Tests for the Bilbao Accelerator Ion Source Test Stand, Proceeding of IPAC'10, Kyoto, Japan, September (2010).
- [7] Dan Faircloth, A. P. Letchford, C. Gabor, M. O. Whitehead, and T. Wood, Rev. Sci. Instrum., 79, 02B717 (2008).